

Article

Digital Calibration for Gain, Time Skew, and Bandwidth Mismatch in Under-Sampling Time-Interleaved System

Min Hu and Pengxing Yi *

School of Mechanical Science and Engineering, Huazhong University of Science and Technology, Wuhan 430074, China

* Correspondence: pxyi@hust.edu.cn; Tel.: +86-27-8755-7415

Abstract: This paper presents an all-digital background calibration method for gain, time skew, and bandwidth mismatch in M -channel under-sampling time-interleaved analog-to-digital converters (TI-ADCs) systems. Firstly, the characteristics of offset, gain, time skew, and bandwidth mismatch on the TI-ADCs system are analyzed. Secondly, a parameter vector is constructed to correct gain, time skew, and bandwidth mismatch. Then, the constructed parameter vector is calculated with the bandpass fractional delay filter and least squares (LS) algorithm. Based on the bandpass fractional delay filter, the proposed technique can work for ultra-high frequency signals. Additionally, the constructed parameter vector has a smaller number of filter taps than the derivative filter or Hilbert filter. Therefore, fewer computing resources are used to correct the input signal after obtaining the proposed parameter vector. Finally, there are matrix inversions in the LS algorithm. Additionally, implementing matrix inversion within FPGA is complex. For this reason, solving a system of linear equations is used to replace matrix inversions. The LS algorithm is affected by quantization error and white Gaussian noise. The simulation results verify the effectiveness of the proposed algorithm when the SNR of sub-ADC is from 30 dB to 100 dB or the ENOB of sub-ADC is from 5-bit to 16-bit. They show that the proposed algorithm is not limited by the first sub-ADC Nyquist. Additionally, the measurement results show that the proposed method is effective in the actual time-Interleaved system.



Citation: Hu, M.; Yi, P. Digital Calibration for Gain, Time Skew, and Bandwidth Mismatch in Under-Sampling Time-Interleaved System. *Appl. Sci.* **2022**, *12*, 11029. <https://doi.org/10.3390/app122111029>

Academic Editor: Antonio Fernández-Caballero

Received: 27 September 2022

Accepted: 28 October 2022

Published: 31 October 2022

Publisher's Note: MDPI stays neutral with regard to jurisdictional claims in published maps and institutional affiliations.



Copyright: © 2022 by the authors. Licensee MDPI, Basel, Switzerland. This article is an open access article distributed under the terms and conditions of the Creative Commons Attribution (CC BY) license (<https://creativecommons.org/licenses/by/4.0/>).

Keywords: digital calibration; gain; time skew; bandwidth mismatch; under-sampling; least squares

1. Introduction

In modern communication systems, analog-to-digital converters play an important role. They can convert analog signals to digital signals. Among many kinds of analog-to-digital converters (ADCs), the successive-approximation-register (SAR) ADCs are widely accepted due to their low design complexity. Additionally, the newest single-channel SAR analog-to-digital converter (ADC) operates at 12-bit, 1 GS/s [1]. However, the center frequency of the 5G signal is above 1 GHz, which requires a higher sampling rate for the SAR ADC.

In 1980, a special framework of ADC, which is named time-interleaved analog-to-digital converters (TI-ADCs) has been proposed by W.C. Black [2]. Based on this special framework, an M -channel TI-ADCs system can achieve a sampling rate M times faster than a single channel. Nevertheless, there are some mismatches between different sub-ADCs in the special framework. Additionally, the mismatches include offset, gain, time skew, and bandwidth mismatch [3–6]. In the TI-ADCs system, the mismatches lead to a discrepancy between the actual output digital signal and the ideal output digital signal. Therefore, these mismatches should be estimated and corrected to improve the performance of the TI-ADCs system.

Background calibration [7–18] and foreground calibration [19–22] are two of the categories for the calibration techniques of TI-ADCs. Foreground calibration means calibrating mismatches before sampling the target signal in the TI-ADCs system. Additionally, these

techniques generally calibrate mismatches by a specific signal [19–21]. The whole calibration process is completed before the input signal is sampled. If the changes in pressure, volume, and temperature lead to changes in mismatches after the foreground calibrations are completed, the changed mismatches will not be calibrated. Moreover, the performance of foreground calibration is affected by the accuracy of the specific signal. Based on these reasons, this article aims to research a background calibration in the TI-ADCs system.

The background calibration can be divided into the following two steps: mismatches estimation and mismatches correction. The offset and gain can be corrected with digital adders and digital multipliers, respectively [16]. The time skew can be corrected by adjusting the sampling clock [8,9] or digitally controlled variable delay lines (VDLs) [15] or the derivative filter [10,11,14,16,17] or the adaptive filter [13]. When the time skew is corrected by adjusting the sampling clock, the effect of the correction depends on the accuracy of the adjustment. Therefore, high-precision circuits are required to adjust the sampling clock in the ultra-high-speed TI-ADCs system. The time skew can be corrected with kinds of filters to avoid demanding hardware circuits. However, the derivative filter is applied to correct the time skew, which limits the size of the time skew [13]. The bandwidth mismatch can be corrected by adjusting the sample and hold circuit [6] or the cascaded derivative filter or the adaptive filter [4].

Compared with digital correction technologies, using analog circuits to correct time skew and bandwidth mismatch does not involve many digital calculation modules. Therefore, analog correction technologies are suitable for on-chip TI-ADCs. However, they require state-of-the-art manufacturing technologies because of the increasing frequency of the input signals.

Figure 1 is the conceptual graph of an M -channel time-interleaved analog-to-digital conversion system. Here, CLK_i is the sample clock of the sub-ADC, M is the number of channels, and Φ_i is the initial phase of CLK_i . o_i , g_i , τ_i , and $H_{\omega_i}(j\omega)$ are offset, gain, time skew [7], and bandwidth mismatch [21], respectively. Firstly, the M sub-ADCs convert the input signal into digital signals by a time-interleaved technique [2]. Secondly, the digital signals are transmitted into the field-programmable gate array (FPGA). Then, the digital signals are buffered in the FPGA. Finally, the reorganization of the signals is completed in the FPGA or computer. There are many mathematical operation modules in the FPGA or computer. Additionally, these mathematical operation modules can be used for digital calibration methods. Therefore, it is of practical significance to study digital calibration methods to reduce the accuracy requirements of analog circuits.

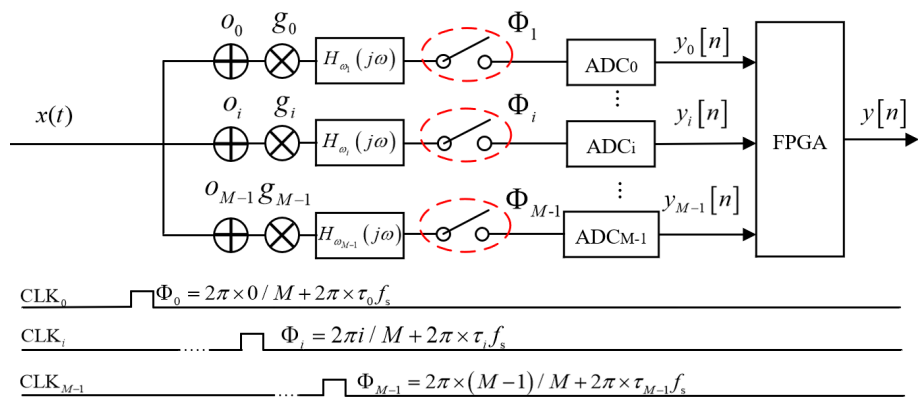


Figure 1. Conceptual graph of an M -channel time-interleaved analog-to-digital conversion system.

In the continuous-time wide-sense stationary (WSS) signal, the offset can be estimated using the mean, and the gain can be estimated using the standard deviation. The estimation of time skew and bandwidth mismatch can be divided into three strategies: (a) reference ADC [9]; (b) autocorrelation of the signal [13]; (c) fractional delay filter. There are the following three disadvantages to the strategy of reference ADC: (1) additional reference

ADC significantly increases power consumption and hardware overhead [23]. (2) The reference channel will generate additional spurs by changing the input impedance of the TI-ADC [24]. (3) alternating the reference ADC with a single comparator can result in a slow convergence [25]. These disadvantages do not exist in the all-digital calibration strategies of autocorrelation of the signal or fractional delay filter. However, there is high computational complexity, a limitation in the first sub-ADC bandwidth, and slow operational speed for all-digital calibration strategies, which adopt autocorrelation of the signal or fractional delay filter.

A digital calibration technique for timing skew is proposed in the reference [26]. However, this technique cannot deal with the gain mismatch. In this paper, a new parameter vector is proposed to correct gain, time skew, and bandwidth mismatch simultaneously. Firstly, compared with the techniques calibrating time skew by the Taylor series [10,13], the proposed approach enables a wide range of time skew mismatch compensation. Secondly, the proposed parameter vector has a smaller number of filter taps than the derivative filter [10,13] or Hilbert filter [27]. Therefore, fewer computing resources are used to correct the input signal after obtaining the proposed parameter vector. Then, ref. [16] limits its application to the TI-ADCs with specific channel numbers to ensure there are Hadamard transforms for the given channel number. However, the proposed algorithm is not limited by the number of channels. Finally, the proposed parameter vector is estimated with the bandpass fractional delay filter and least squares (LS) algorithm. Based on the bandpass fractional delay filter, the proposed technique can work for ultra-high frequency signals. Additionally, there are matrix inversions in the LS algorithm. The implementation of matrix inversion within FPGA is complex. Therefore, solving a system of linear equations is used to replace matrix inversions.

The structure of this paper has the following parts: Section 2 describes the TI-ADCs model, the characteristics of offset, gain, time skew, and bandwidth mismatch, and the correction of these mismatches. Section 3 explains how to apply the LS algorithm to estimate gain, time skew, and bandwidth mismatch. Section 4 explains the bandpass fractional delay filter and the alternative method of the matrix inversion and validates the proposed technique by showing results from simulation and measurement. In the end, Section 5 concludes this article.

2. System Model and the Correction of Offset, Gain, Time Skew, and Bandwidth Mismatch

2.1. System Model

Figure 1 shows the abstract view of an M -channel time-interleaved analog-to-digital conversion system. Additionally, ADC_0 is assumed as the reference ADC. When there is an offset, gain, and time skew in the TI-ADCs system, the discrete-time Fourier Transform (DTFT) of the i -th channel output is represented as follows [7]:

$$Y_i(j\omega) = g_i e^{-j\omega\Delta\tau_i} X_i(j\omega) + o_i, \quad (1)$$

here $X_i(j\omega)$, o_i , g_i and $\Delta\tau_i$ are respectively the DTFT of the input signal before distortion, the offset, the gain, and the time skew in the i -th channel.

The inverse discrete-time Fourier transform (IDTFT) of $e^{-j\omega\Delta\tau_i}$ can be expressed as follows:

$$h_{\Delta\tau_i}[k] = \frac{\sin\left(\pi\left(k - \frac{\Delta\tau_i}{T_s}\right)\right)}{\pi\left(k - \frac{\Delta\tau_i}{T_s}\right)}. \quad (2)$$

When there are bandwidth mismatches in this TI-ADCs system, the DTFT of the output in the i -th channel can be represented as follows:

$$Y_i(j\omega) = g_i e^{-j\omega\Delta\tau_i} H_{\omega_i}(j\omega) X_i(j\omega) + o_i, \quad (3)$$

where $H_{\omega_i}(j\omega)$ is the frequency response of bandwidth mismatch. Additionally, the IDTFT of $H_{\omega_i}(j\omega)$ can be approximated by a single-pole low-pass filter as follows [21]:

$$H_{\omega_i}(j\omega) = \frac{1}{1 + j\frac{\omega}{\omega_{bi}}}, \quad (4)$$

where ω_{bi} is the cutoff frequency of the sample and hold circuit of the i -th channel.

2.2. Correction of Offset, Gain, Time Skew, and Bandwidth Mismatch

ADC_0 is used as the reference ADC. Additionally, offset, gain, time skew, and bandwidth mismatch of the reference ADC are assumed to be zero. Hence, Equation (3) can be rewritten as follows:

$$Y_i(j\omega) = \Delta g_i e^{-j\omega\Delta\tau_i} H_{\Delta\omega_i}(j\omega) X_i(j\omega) + \Delta o_i, \quad (5)$$

here Δo_i , Δg_i and $\Delta\tau_i$ are, respectively, the offset, gain, and time skew relative to the reference channel. Additionally, $H_{\Delta\omega_i}(j\omega)$ can be expressed as follows:

$$H_{\Delta\omega_i}(j\omega) = \frac{1 + j\frac{\omega}{\omega_{br}}}{1 + j\frac{\omega}{\omega_{bi}}}, \quad (6)$$

where ω_{br} is the cutoff frequency of the sample and the hold circuit of the reference channel.

In the TI-ADCs system, offset and gain can be corrected by the adder and multiplier, respectively. Additionally, Figure 2 is the proposed structure of correction offset and gain. In Figure 2, \tilde{o}_i is the value of estimating the offset, \tilde{g}_i is the value of estimation of the gain and $y_{icalo,g}[n]$ is the output after calibrating the offset and the gain.

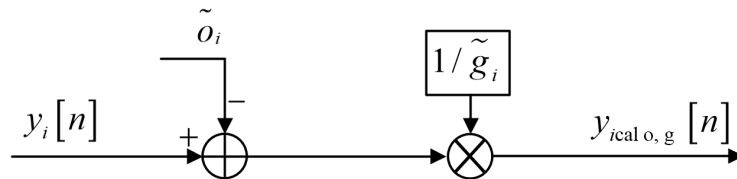


Figure 2. Proposed structure of correction offset and gain.

When the filter is used to correct the time skew and the bandwidth mismatch at the same time, the frequency response of the filter can be represented as follows:

$$H_{\Delta\tau_i,\Delta\omega_i}(j\omega) = e^{j\omega\tau} \times \frac{1 + j\frac{\omega}{\omega_{bi}}}{1 + j\frac{\omega}{\omega_{br}}}. \quad (7)$$

The IDTFT of $H_{\Delta\tau_i,\Delta\omega_i}(j\omega)$ can be expressed as $h_{\Delta\tau_i,\Delta\omega_i}[k]$. When there are time skews and bandwidth mismatches in the TI-ADCs system, the correction of these mismatches can be expressed as follows:

$$y_{icalo,g,\tau,\omega}[n] = y_{icalo,g}[n] * h_{\Delta\tau_i,\Delta\omega_i}[k]. \quad (8)$$

Here $*$ is the convolution and $y_{icalo,g,\tau,\omega}[n]$ is the output after calibrating the offset, gain, time skew, and bandwidth mismatch. When $h_{\Delta\tau_i,\Delta\omega_i}[k]$ is an N -tap filter, Equation (8) can be rewritten as follows:

$$y_{icalo,g,\tau,\omega}[n] = \begin{cases} \sum_{k=1}^N y_{icalo,g}\left[n - k + 1 + \frac{N}{2}\right] \times h_{\Delta\tau_i,\Delta\omega_i}[k], & \text{when } N \text{ is even.} \\ \sum_{k=1}^N y_{icalo,g}\left[n - k + 1 + \frac{N-1}{2}\right] \times h_{\Delta\tau_i,\Delta\omega_i}[k], & \text{when } N \text{ is odd.} \end{cases} \quad (9)$$

Based on Equation (9), Figure 3 shows the proposed structure of correction time skew and bandwidth mismatch. Additionally, N is even in Figure 3. Based on Figures 2 and 3, the offset, gain, time skew, and bandwidth mismatch can be corrected.

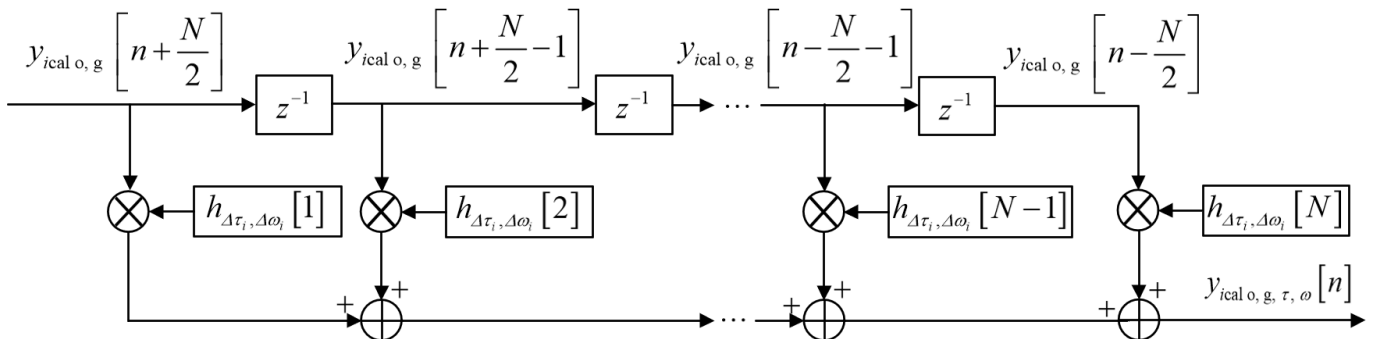


Figure 3. Proposed structure of correction time skew and bandwidth mismatch.

3. The Extraction of Offset, Gain, Time Skew, and Bandwidth Mismatch

The input signals in the proposed methods are wide-sense stationary. Hence, the statistical characteristics for each sub-ADC output are the same when there is no mismatch in the TI-ADCs system.

3.1. The Extraction of the Offset and Gain

The offset can be extracted from the following formula:

$$\tilde{o}_i = \frac{\sum_{n=1}^{L_o} y_i[n]}{L_o}, \quad (10)$$

where the offset \tilde{o}_i is approximated by the L_o samples of the i -th sub-ADC. Similarly, the gain can be extracted from the following formula [28]:

$$\tilde{g}_i = \sqrt{\frac{\sum_{n=1}^{L_g} y_i^2[n]}{L_g}}, \quad (11)$$

here the gain \tilde{g}_i is approximated by the L_g samples of the i -th sub-ADC.

Based on Equations (10) and (11), the offset and gain can be estimated. However, the process of estimating the gain in Equation (11) involves many multiplications. When the offset has been calibrated, Equation (5) can be rewritten as follows:

$$Y_{\text{ical } o}(j\omega) = \Delta g_i e^{-j\omega\Delta\tau_i} H_{\Delta\omega_i}(j\omega) X_i(j\omega). \quad (12)$$

Based on the Equations (8) and (12), the correction of the gain, time skew, and bandwidth mismatch can be represented as follows:

$$y_{\text{ical } o, g, \tau, \omega}[n] = y_{\text{ical } o}[n] * h_{\Delta g_i, \Delta\tau_i, \Delta\omega_i}[k], \quad (13)$$

where $h_{\Delta g_i, \Delta\tau_i, \Delta\omega_i}[k]$ can be obtained with the following:

$$h_{\Delta g_i, \Delta\tau_i, \Delta\omega_i}[n] = \frac{h_{\Delta\tau_i, \Delta\omega_i}[n]}{\Delta g_i}. \quad (14)$$

3.2. The Extraction of the Gain, Time Skew and Bandwidth Mismatch

To extract the gain, time skew, and bandwidth mismatch, the fractional delay filter is introduced to construct the reference. Additionally, the reference of the i -th channel can be represented as follows:

$$y_{ri}[n] = y_0[n] * h_{ri}[k], \quad (15)$$

Here $y_0[n]$ is the output of ADC₀. And the DTFT of $h_{ri}[k]$ is represented as follows:

$$H_{ri}(j\omega) = e^{-j\omega T_s \frac{i}{M}}, \quad (16)$$

where M is the number of channels. Hence, the error function of estimation gain, time skew, and bandwidth mismatch can be represented as follows:

$$e_i[n] = y_0[n] * h_{ri}[k] - y_{ical\ o}[n] * h_{\Delta g_i, \Delta \tau_i, \Delta \omega_i}[k], \quad (17)$$

here $h_{\Delta g_i, \Delta \tau_i, \Delta \omega_i}[k]$ is the coefficients of an N -tap filter. And N is even. Hence, Equation (17) can be represented as follows:

$$e_i[n] = y_{ri}[n] - \sum_{k=1}^N y_{ical\ o}\left[n - k + 1 + \frac{N}{2}\right] \times h_{\Delta g_i, \Delta \tau_i, \Delta \omega_i}[k]. \quad (18)$$

The minimum value of $\sum(e_i[n])^2$ is obtained by the least square method. Hence, $h_{\Delta g_i, \Delta \tau_i, \Delta \omega_i}[k]$ can be represented as follows:

$$h_{\Delta g_i, \Delta \tau_i, \Delta \omega_i}[k] = \left(\mathbf{y}_{ical\ o}^T \mathbf{y}_{ical\ o}\right)^{-1} \mathbf{y}_{ical\ o}^T \mathbf{y}_{ri}, \quad (19)$$

where T is represented as matrix transposition and $^{-1}$ is represented as matrix inversion. Additionally, \mathbf{y}_{ical} can be represented as follows:

$$\mathbf{y}_{ical\ o} = \begin{bmatrix} y_{ical\ o}\left[1 + \frac{N}{2}\right] & \cdots & y_{ical\ o}\left[N + \frac{N}{2}\right] \\ \vdots & \ddots & \vdots \\ y_{ical\ o}\left[L_s + \frac{N}{2}\right] & \cdots & y_{ical\ o}\left[L_s + N + \frac{N}{2}\right] \end{bmatrix}_{L_s \times N}. \quad (20)$$

Here L_s is the number of samples. Additionally, \mathbf{y}_{ri} can be represented as follows:

$$\mathbf{y}_{ri} = \begin{bmatrix} y_{ical\ o}\left[1 + \frac{N}{2}\right] \\ \vdots \\ y_{ical\ o}\left[L_s + \frac{N}{2}\right] \end{bmatrix}_{L_s \times 1}. \quad (21)$$

Hence, the gain, time skew, and bandwidth mismatch can be estimated with Equations (19)–(21). Based on Equations (10) and (19), Figures 2 and 3, the calibration of offset, gain, time skew, and bandwidth mismatch can be shown in Figure 4.

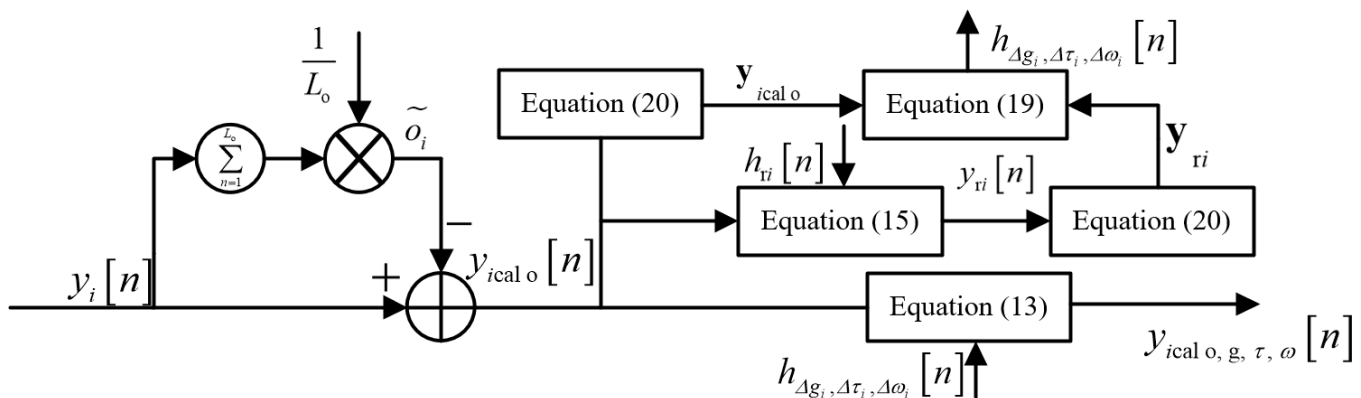


Figure 4. Proposed structure of correction of the offset, gain, time skew, and bandwidth mismatch.

4. Test Verification

In summary, the offset can be extracted with Equation (10). Figure 4 shows how to calibrate gain, time skew, and bandwidth mismatch.

4.1. A Fixed Fractional Delay Filter

The proposed method adopts the fractional delay filters to estimate the gain, time skew, and bandwidth mismatch in each channel. The fractional delay filters are used in each sub-ADC. Therefore, the input signal is limited to the first Nyquist bandwidth of the sub-ADC. To make the proposed algorithm work for the high Nyquist bandwidth of the sub-ADC in the TI-ADCs system, the fractional delay filters should be effective in high sub-ADC Nyquist bandwidth.

When the bandpass (BP) signals are in the N_{BP} -th Nyquist bandwidth, the frequency can be expressed as follows:

$$(N_{BP} - 1) \times \frac{f_s}{2} < f_L < |f| < f_H < N_{BP} \times \frac{f_s}{2}. \quad (22)$$

Here $N_{BP} \geq 1$, f_L , and f_H are the low and high cutoff frequencies of the signal, respectively. Additionally, f_s is the sampling frequency of sub-ADC.

The BP signal is constructed by the sum of two complex signals of $x^+(t)$ and $x^-(t)$. Therefore, the frequency response of the complex signals can be respectively represented as $X^+(f)$ and $X^-(f)$. According to the band-pass sampling theory, the original spectrum of the band-pass signal can be folded back to the baseband in the under-sampled TI-ADC converter whose sampling frequency conforms to the Nyquist criterion. In the odd-order Nyquist band, the baseband spectrum of the under-sampling signal has the same shape as the original spectrum. Additionally, the baseband spectrum of even order NB input signal is reversed. In the odd-order Nyquist band, $X(f)$ can be represented as follows:

$$\begin{aligned} X(f) &= X^+(f) + X^-(f) \\ &= T_s Y^+(f - n_n f_s) + T_s Y^-(f + n_n f_s). \end{aligned} \quad (23)$$

Here, $Y^+(f)$ and $Y^-(f)$ is the output of $X^+(f)$ and $X^-(f)$, respectively. Furthermore, n_n can be obtained as follows:

$$n_n = \left\lfloor \frac{N_{BP}}{2} \right\rfloor. \quad (24)$$

where the input signal is the N_{BP} -th Nyquist bandwidth and $\lfloor N_{BP}/2 \rfloor$ is the result of rounding down $N_{BP}/2$. Therefore, the inverse fast Fourier transform (IFFT) of $X(f)$ can be expressed as

$$x(t) = T_s y^+(t) e^{j2\pi n_n f_s t} + T_s y^-(t) e^{-j2\pi n_n f_s t}. \quad (25)$$

According to the Euler formula, $x(t)$ can be rewritten as follows:

$$\begin{aligned} x(t) &= T_s \cos(2\pi n_n f_s t)(y^+(t) + y^-(t)) \\ &\quad + jT_s \sin(2\pi n_n f_s t)(y^+(t) - y^-(t)). \end{aligned} \quad (26)$$

In the time domain, $y^+(t)$ and $y^-(t)$ can be obtained as follows:

$$\begin{aligned} y^+(t) &= \frac{y(t) + jy_h(t)}{2}, \\ y^-(t) &= \frac{y(t) - jy_h(t)}{2}. \end{aligned} \quad (27)$$

According to Equation (27), the reference of the i -th channel can be represented as follows:

$$\begin{aligned} x_0\left(t + \frac{i}{Mf_s}\right) &= T_s \cos\left(2\pi n_n f_s \left(t + \frac{i}{Mf_s}\right)\right) \left(y_0\left(t + \frac{i}{Mf_s}\right)\right) \\ &\quad + jT_s \sin\left(2\pi n_n f_s \left(t + \frac{i}{Mf_s}\right)\right) \left(jy_{h0}\left(t + \frac{i}{Mf_s}\right)\right). \end{aligned} \quad (28)$$

Therefore, the DFT of Equation (28) can be expressed as follows:

$$\begin{aligned} x_0\left[n + \frac{i}{Mf_s}\right] &= \cos\left[2\pi n_n \left(n + \frac{i}{M}\right)\right] \left(y_0\left[n + \frac{i}{Mf_s}\right]\right) \\ &\quad - \sin\left[2\pi n_n \left(n + \frac{i}{M}\right)\right] \left(y_{h0}\left[n + \frac{i}{Mf_s}\right]\right), \end{aligned} \quad (29)$$

where, $y_0[n + i/Mf_s]$ can be represented as follows:

$$y_0\left[n + \frac{i}{Mf_s}\right] = y_0[n] * h_{ri}[n], \quad (30)$$

And $y_{h0}[n + i/Mf_s]$ can be represented as follows:

$$y_{h0}\left[n + \frac{i}{Mf_s}\right] = y_0[n] * h_{ri}[n] * h_h[n]. \quad (31)$$

In the even Nyquist bands, the DFT of $x_i(t + i/Mf_s)$ can be expressed as follows:

$$\begin{aligned} x_0\left[n + \frac{i}{Mf_s}\right] &= \cos\left[2\pi n_n \left(n + \frac{i}{M}\right)\right] \left(y_0\left[n + \frac{i}{Mf_s}\right]\right) \\ &\quad + \sin\left[2\pi n_n \left(n + \frac{i}{M}\right)\right] \left(y_{h0}\left[n + \frac{i}{Mf_s}\right]\right). \end{aligned} \quad (32)$$

Figure 5 shows the reference generation of the TI-ADC system with BP signal input. The IDFT of Hilbert filter frequency response can be expressed as follows:

$$h_h[n] = \begin{cases} \frac{2}{\pi} \times \frac{\sin^2(\frac{n\pi}{2})}{n} & (n \neq 0) \\ 0 & (n = 0) \end{cases}. \quad (33)$$

Additionally, the causal filters' coefficients are obtained by windowing Equation (33).

4.2. Simulation Result

The signal-to-noise distortion ratio (SNDR) is a metric that describes the signal performance. Additionally, SNDR can be calculated by the following:

$$\text{SNDR} = 10 \lg \left(\frac{P_{\text{Signal}}}{P_{\text{Noise}} + P_{\text{Distortion}}} \right) \quad (34)$$

where P_{Signal} is the power of the ideal signal, P_{Noise} is the power of the noise signal, and $P_{\text{Distortion}}$ is the spurious power of the output signal. In the TI-ADCs system, the presence of mismatches leads to an increase in P_{Noise} . When P_{Signal} and P_{Noise} are fixed, the smaller the calibration error, the higher the SNDR. Therefore, the SNDR is applied to evaluate the effect of error calibration.

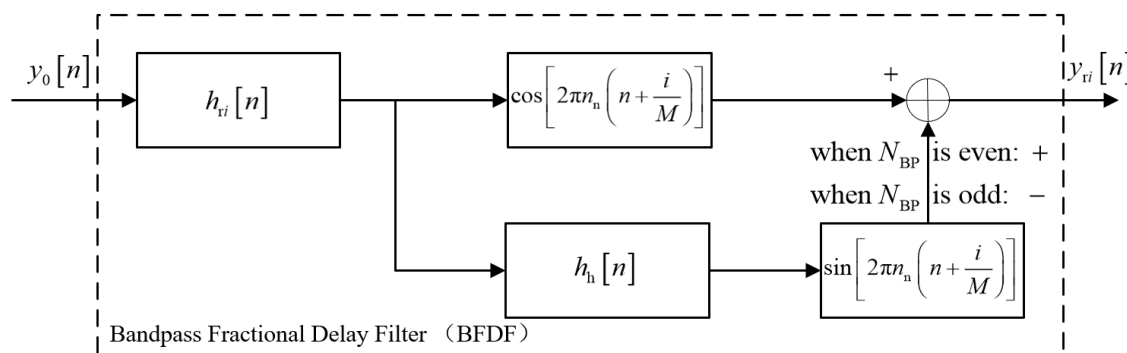


Figure 5. Bandpass fractional delay filter.

The calibration of offset is simpler than other mismatches. Hence, the offset is set to 0 in the simulation tests. The 12-bit 8 GS/s 8-channel TI-ADCs simulation system is established according to Equation (3) with MATLAB. Additionally, the mismatches of the simulation model are shown in Table 1. Moreover, the parameters of the bandpass fractional filters are shown in Table 2. Additionally, the number of taps of $h_{\Delta g_i, \Delta \tau_i, \Delta \omega_i}[k]$ is 73. In the 12-bit 8 GS/s 8-channel TI-ADCs simulation system, the SNDR of the input signal before sampling is 60 dB because of the Gaussian white noise in each channel.

Table 1. The mismatches of the TI-ADCs simulation system.

Sub-ADC Number	Offset	Gain	Time Skew	Bandwidth
1	0	1	0	$4 \times f_s$
2	0	1	0	$1 \times f_s$
3	0	1	0	$2 \times f_s$
4	0	1	0	$3 \times f_s$
5	0	1	0	$1 \times f_s$
6	0	1	0	$2 \times f_s$
7	0	1	0	$3 \times f_s$
8	0	1	0	$3 \times f_s$

Table 2. Parameters for the filters.

Parameter	Filter Design Method	Number of Taps
Fractional delay filters	Blackman Window	73
Hilbert transform filters	Blackman Window	73

Figure 6 shows the values of SNDR and spurious-free dynamic range (SFDR) for sinusoidal signals with the different frequencies of the first Nyquist bandwidth. The frequency range is limited within 0.05–0.42 GHz. Additionally, the frequency spacing between two single-tone sinusoidal signals is 0.01 GHz. Where f_c is the sampling frequency of sub-ADC. In Figure 6a, the SNDR is stable above 65 dB in the test frequency range. Additionally, the SFDR is stable above 80 dB in Figure 6b.

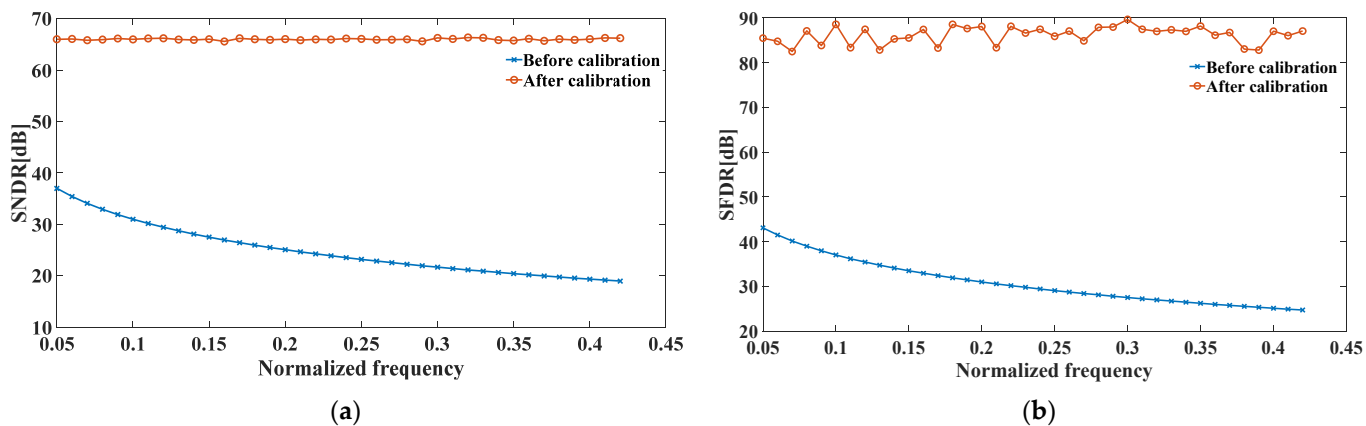


Figure 6. Performances of bandwidth mismatch calibration with the proposed method. (a) The SNDR of TI-ADCs with different frequencies; (b) the SFDR of TI-ADC with different frequencies.

The mismatches shown in Table 3 are set to verify that the proposed methods are still effective when there are gain, time skew, and bandwidth mismatch at the same time. The frequency range is limited within 0.05–0.42 GHz. Where f_c is the frequency of sub-ADC, and f_s is the frequency of the TI-ADCs system. Additionally, Figure 6 shows the SNDR and SFDR before and after calibration. It can be seen from Figure 7 that the proposed calibration method still has a good effect in the cases of gain, time skew, and bandwidth mismatch. The SNDR before calibration does not exceed 20 dB. Additionally, the SNDR is above 65 dB after calibration. Therefore, the value of SNDR is improved by at least 45 dB after calibration. Moreover, the value of SFDR is above 80 dB after calibration.

Table 3. The mismatches of the TI-ADCs system.

Sub-ADC Number	Offset	Gain	Time Skew	Bandwidth
1	0.000	1.000	0.000	$4.000 \times f_s$
2	0.000	1.400	± 0.500	$1.000 \times f_s$
3	0.000	1.300	± 0.200	$2.000 \times f_s$
4	0.000	1.200	± 0.100	$3.000 \times f_s$
5	0.000	1.100	± 0.400	$1.000 \times f_s$
6	0.000	1.200	± 0.300	$2.000 \times f_s$
7	0.000	1.300	± 0.100	$3.000 \times f_s$
8	0.000	1.100	± 0.200	$3.000 \times f_s$

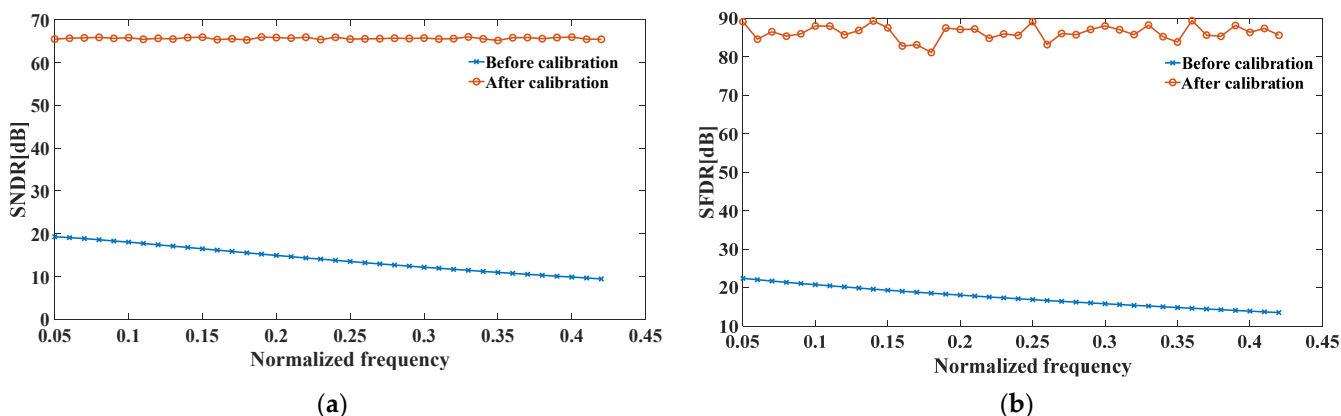


Figure 7. Performances of the proposed method. (a) The SNDR of TI-ADCs with different frequencies; (b) the SFDR of TI-ADC with different frequencies.

Figures 8 and 9 show the calibration performance within the second and third Nyquist bandwidths of the sub-ADC, respectively. Additionally, the frequency ranges are limited within 0.55–0.92 GHz and 1.05–1.42 GHz, respectively. The offset, gain, time skew, and bandwidth mismatch of the TI-ADCs system are shown in Table 3.

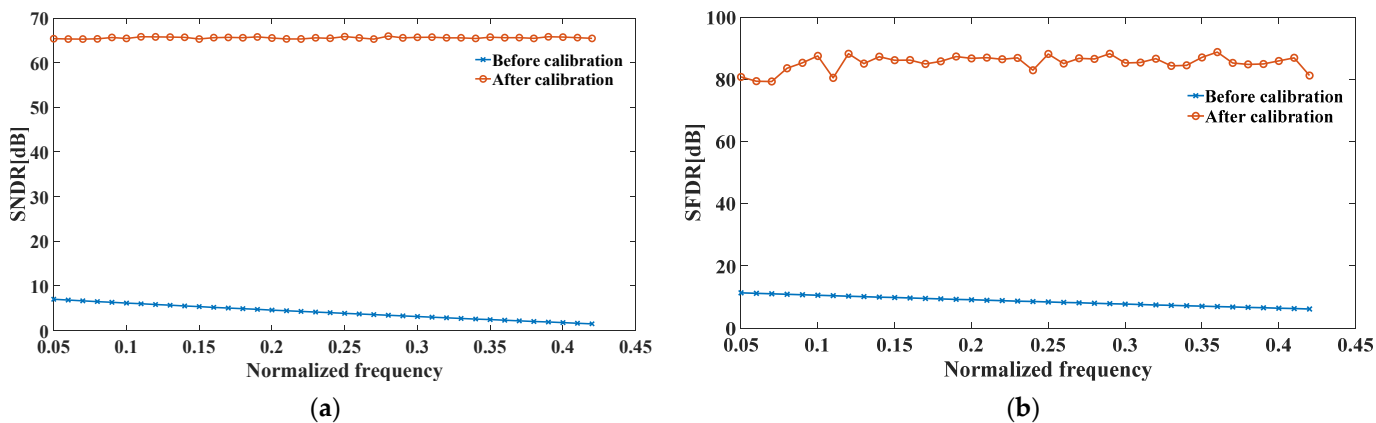


Figure 8. Performances of the proposed method in the second Nyquist bandwidth of the sub-ADC. (a) The SNDR of TI-ADCs with different frequencies; (b) the SFDR of TI-ADC with different frequencies.

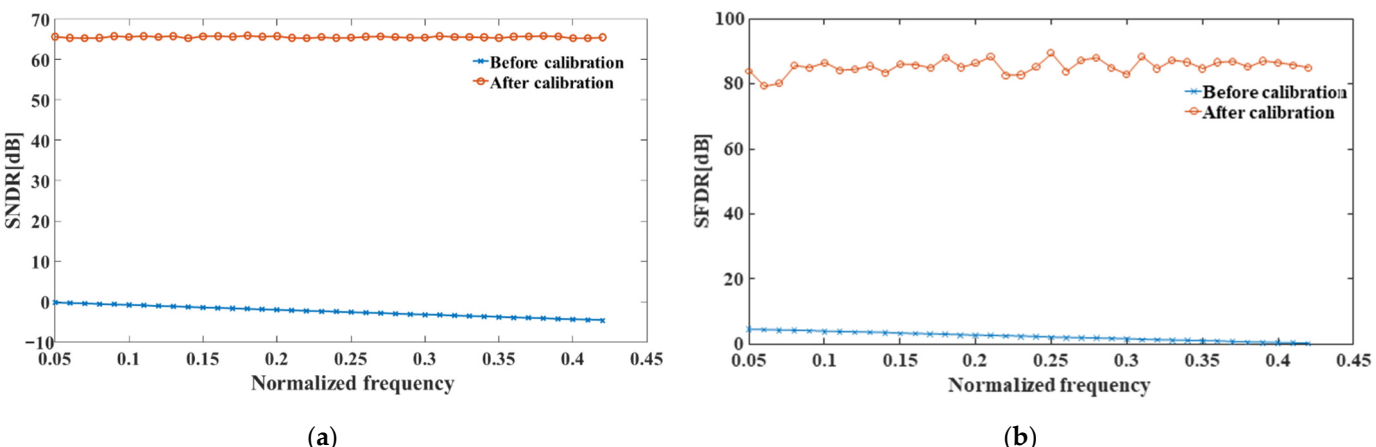


Figure 9. Performances of the proposed method in the third Nyquist bandwidth of the sub-ADC. (a) The SNDR of TI-ADCs with different frequencies; (b) the SFDR of TI-ADC with different frequencies.

It can be seen from Figures 7–9 that the SNDR and SFDR of the TI-ADCs system decrease with the increase in the input signal frequency at the same gain, time skew, and bandwidth mismatch. Figures 8 and 9 show that even if the input signal is not located in the first Nyquist bandwidth of the sub-ADC, the proposed methods still have a good calibration effect. Furthermore, Figures 7–9 show that the proposed methods are effective for bandpass signals with different Nyquist bandwidths. Additionally, the SNDR is above 65 dB and the SFDR is above 80 dB in the first, second, and third Nyquist frequency bands. Therefore, the frequency of the input signal has relatively little effect on the proposed technique.

Figure 10 shows the frequency spectrums of the multi-tone signal before and after calibration. Where the frequencies of the multi-tone signal are [2.30 GHz, 2.42 GHz, 2.54 GHz, 2.66 GHz, 2.78 GHz]. Figure 10a shows the frequency spectrum of the TI-ADCs system before calibration. Where the offset, gain, time skew, and bandwidth mismatch are shown in Table 3. The performance of the TI-ADCs system shown in Figure 10a is poor. Where the SNDR is -2.77 dB and the SFDR is -17.28 dB. Additionally, the performance of the TI-ADCs system is well-improved after calibration. In Figure 10b, the SNDR is 60.19 dB and the SFDR is 75.53 dB. Therefore, the SNDR is improved by 62.96 dB, and the SFDR

is improved by 92.81 dB. Figure 10 shows that the proposed calibration algorithm is still effective for multi-tone bandpass signals with high sub-ADC Nyquist bandwidth.

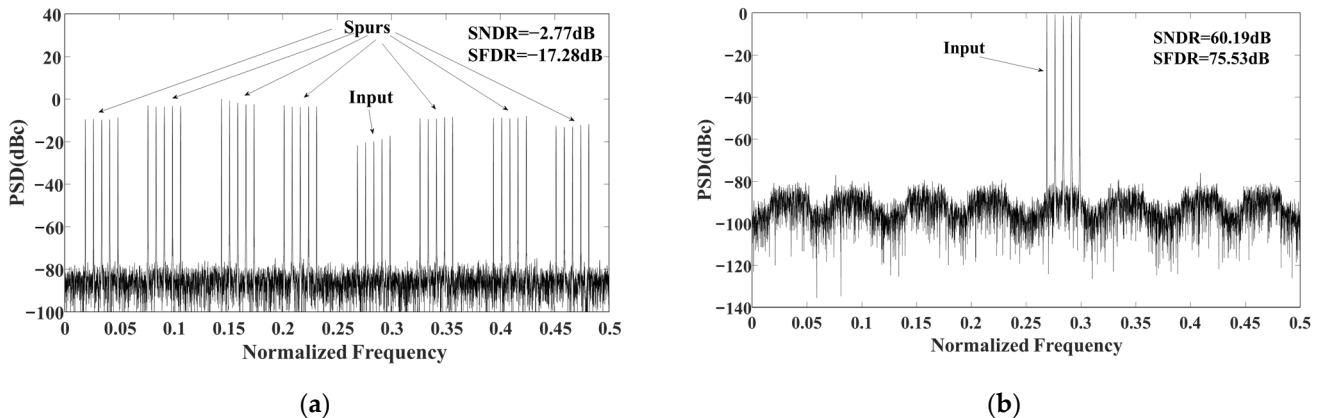


Figure 10. Performances of mismatches calibration for a multi-tone signal. (a) Before calibration; (b) after calibration.

There are matrix inversions in the LS algorithm. Additionally, the implementation of matrix inversion in FPGA is complex. Therefore, Equation (19) is rewritten as follows:

$$\left(\mathbf{y}_{\text{ical o}}^T \mathbf{y}_{\text{ical o}} \right) h_{\Delta g_i, \Delta \tau_i, \Delta \omega_i}[k] = \mathbf{y}_{\text{ical o}}^T \mathbf{y}_{ri}. \quad (35)$$

Hence, a system of linear equations can be constructed as follows:

$$\mathbf{A}_{N \times N} h_{\Delta g_i, \Delta \tau_i, \Delta \omega_i}[k] = \mathbf{b}_{N \times 1}. \quad (36)$$

According to Cramer's rule [29], the solution of $h_{\Delta g_i, \Delta \tau_i, \Delta \omega_i}[k]$ requires about $N!(N - 1)(N + 1)$ times of addition and $N!(N + 1)N$ times of multiplication. In this way, the matrix inversion can be avoided when solving $h_{\Delta g_i, \Delta \tau_i, \Delta \omega_i}[k]$. Additionally, the solution of $\mathbf{A}_{N \times N}$ requires about $N(L_s - 1)N$ times of addition and $NL_s N$ times of multiplication. Similarly, the solution of $\mathbf{b}_{N \times 1}$ requires about $N(L_s - 1)$ times of addition and NL_s times of multiplication. Therefore, the estimation in the i -th channel of gain, time skew, and bandwidth mismatch requires about $(N + 1)(N(L_s - 1) + (N - 1)N!) + (M - 1)(L - 1)L_s$ times of addition and $N(N + 1)(L_s + N!) + (M - 1)LL_s$ times of multiplication. Where L is the number of bandpass fractional delay filter taps.

The comparison results of the proposed technique with the prior state-of-the-art are summarized in Table 4. The bandwidth mismatch can be calibrated with the proposed technique. In the reference [13], the calibration of time skew is based on the correlation between channels. However, Equation (36) of reference [13] is established under the necessary condition that the time skew of the adjacent channels is much smaller than the sampling period of the sub-ADC. To summarize, the calibration techniques of reference [13] must meet the necessary condition that the time skew between adjacent channels or compared with the reference channel is much smaller than the sampling period of the sub-ADC. Similarly, there are restrictions on the size of the time skew in the references [30,31]. References [16,27] and this work approach enables a wide range of time skew mismatch compensation. Therefore, references [16,27], and this work have a good effect on the improvement of SNDR and SFDR. Work [13,16,27], and this work needs 1045.5 K, 277.5 K, 720 K, and 128.1 K multiplication modules to estimate time skew, respectively. Additionally, the multiplication modules occupy most of the computing resources in the techniques of time skew estimation or correction. Therefore, it can be considered that the proposed estimation technique in this work has the lowest power consumption. Work [13], work [16], work [27], work [30], work [31], and this work needs 31, 33, 12, 25, 21, and 5 multiplication modules to correct time skew respectively. Therefore, the power consumption of the proposed technique

of correction time skew is far less than techniques [13,16,27,30,31]. ENOB represents the final performance of the TI-ADC system after calibration. Compared with work [16,27], and [30], the proposed technique has the best performance in ENOB. The quantization error is ignored in the work [31]. Therefore, the ENOB after calibration is not compared between work [31] and others.

Table 4. Compared with other techniques.

	[13] Work	[16] Work	[27] Work	[30] Work	[31] Work	This Work
Mismatch types	T	O ¹ , G ² , T ³	O, G, T	T	T	G, T, B ⁴
Blind calibration	Yes	Yes	Yes	Yes	Yes	Yes
Background calibration	Yes	Yes	Yes	Yes	Yes	Yes
Number of sub-ADC channels	4	4	4	4	4	4
Number of bits	12	11	9	10	N/A	12
Input frequency	0.06f _S	0.45f _S	0.18f _S	0.167f _S	0.167f _S	0.167f _S
Convergence time	110 K	10 K	40 K	80 K	3.1 K	N/A
Filter taps with estimation time skew	31	33	12	15	21	73
Samples with estimation time skew	110 K	10 K	40 K	80 K	3.1 K	2 K
The number of adders	(4(M - 1) + L) × 27.5 K	(M - 1)(2M + L - 1) × 2.5 K	((2L + 4)(M - 1) + L - 1) × 10 K	N/A	N/A	(N + 1)(N(L _s - 1) + (N - 1)N!) + (M - 1)(L - 1)
The number of multipliers	(2(M - 1) + L + 1) × 27.5 K	(M - 1)(M + L) × 2.5 K	(2L + 8)(M - 1) × 10 K	N/A	N/A	N(N + 1)(L _s + N!) + (M - 1)L
SNDR improvement (dB)	25.31	43.7	36.55	19	19	38.36
SFDR improvement (dB)	38.52	74	43.72	24.2	24.2	55.75
The effective number of bits (bit)	N/A	9.61	9.02	7.95	11.20	9.72

¹ O is offset. ² G is gain. ³ T is time skew. ⁴ B is bandwidth mismatch. M is the channel number. L is filter length. L_s is the number of samples. N = 5 is the length of the calibration coefficient.

In Equation (19), quantization noise and Gaussian white noise are not considered. Therefore, the calibration of time skew is affected by quantization noise and Gaussian white noise. Figure 11 shows the performances of calibration time skew in a 2-channel 6.4 GS/s TI-ADCS under different white noise levels.

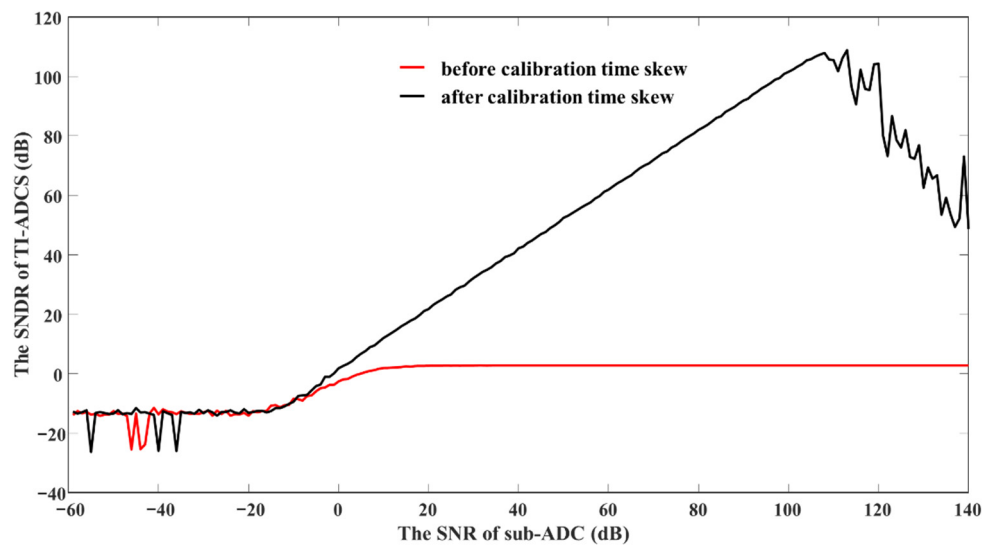


Figure 11. The performance of the proposed technique with different SNR of the input signal.

As shown in Figure 11, there is a positive correlation basically between the SNDR of TI-ADCs and the SNR of sub-ADC when the SNR of sub-ADC is in the range of 0~100 dB. Therefore, the proposed technique can effectively calibrate the gain, time skew, and bandwidth mismatch at the SNR of 0~100 dB. In Figure 12, there is a positive correlation between the SNDR of TI-ADCs and the ENOB of sub-ADC when the ENOB of sub-ADC is in the range of 1 bit~16 bit. It can be seen from Figures 11 and 12 that the proposed technique is effective when the SNR of sub-ADC is in the range of 0~100 dB or the ENOB of sub-ADC is in the range of 1~16 bits.

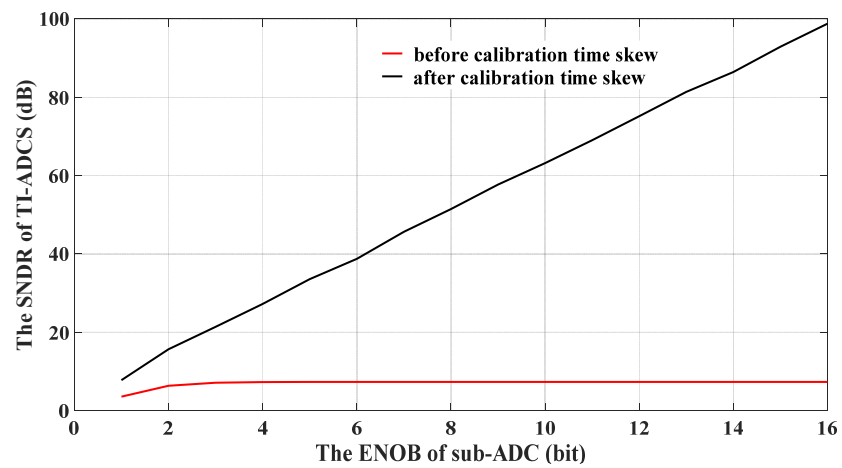


Figure 12. The performance of the proposed technique with different ENOB of the sub-ADC.

The minimum value of $\sum(e_i[n])^2$ is obtained by the least square method. Hence, the cumulative error $\sum(e_i[n])^2$ is affected by quantization error and white Gaussian noise. In Figures 13 and 14, the cumulative errors of the proposed technique are respectively shown under different quantization errors and Gaussian white noise of sub-ADC. It can be seen from Figures 13 and 14 that the cumulative error is stable and approaches 0 when the SNR is greater than 30 dB and the ENOB is greater than 5 bits. It can be concluded from Figures 11–14 that the proposed technique will be affected by the SNR and ENOB. However, the proposed technique has a good effect in the 30~100 dB of SNR or the 5~16 bit of ENOB.

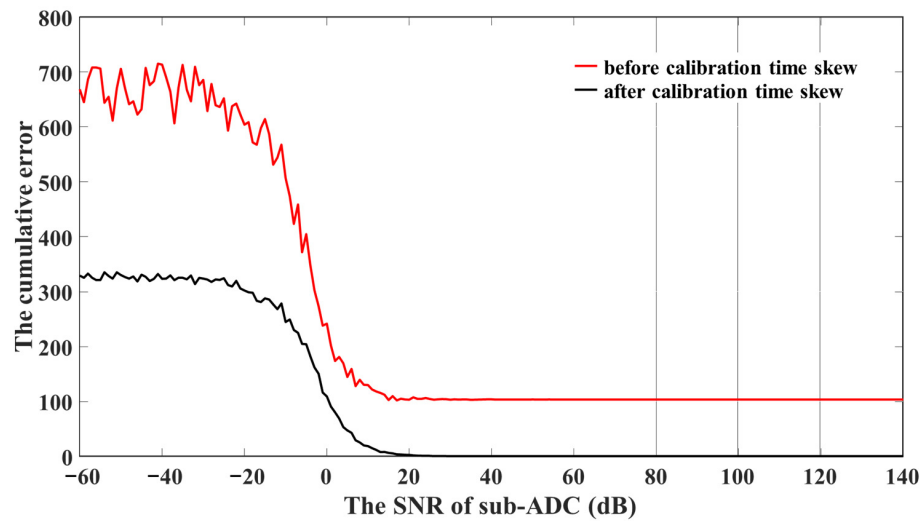


Figure 13. The cumulative errors under different SNR of the sub-ADC in the proposed technique.

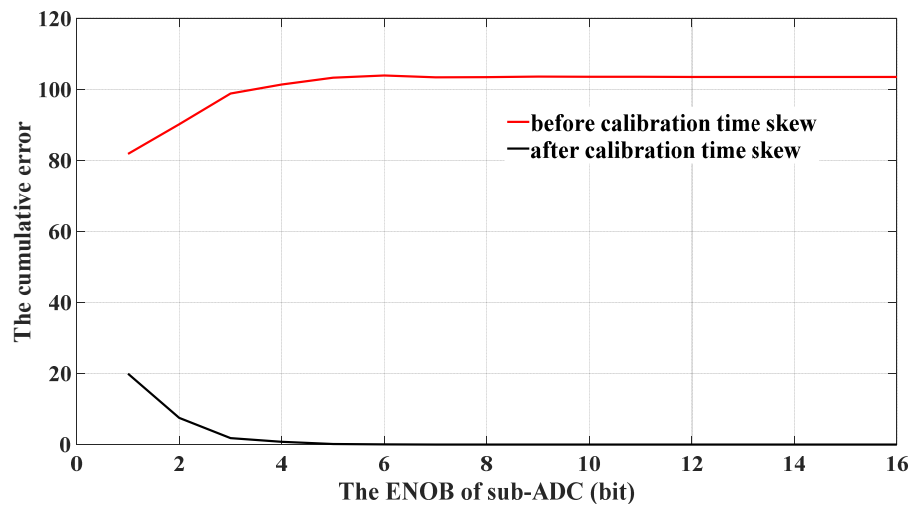


Figure 14. The cumulative errors under different ENOB of the sub-ADC in the proposed technique.

4.3. Measurement Result

A commercial 12-bit 800 Msps 2-channel TI-ADC was used to validate the proposed calibration algorithm under real conditions. The measurement setup is illustrated in Figure 15, and it consists of a signal generator (SDG6032X), a commercial 2-channel TI-ADCs (ADC12DL3200EVM), and a field-programmable gate array (TSWDL3200) for data transmission.

The features of experimental equipment can be shown in Table 5. Figure 16 shows the frequency spectrum before and after calibration. Additionally, the input is a single sinusoidal signal. The frequency of the input signal is 70 MHz. As shown in Figure 16, the SNDR and SFDR are, respectively, 17.15 dB and 17.17 dB. Additionally, the SNDR and SFDR are respectively 43.19 dB and 65.19 dB after calibration by the proposed algorithm. Additionally, it can also be seen from Figure 16 that the spurs of time skew drop below the noise floor. Therefore, the measurement result demonstrates that the proposed method is effective against time skew.

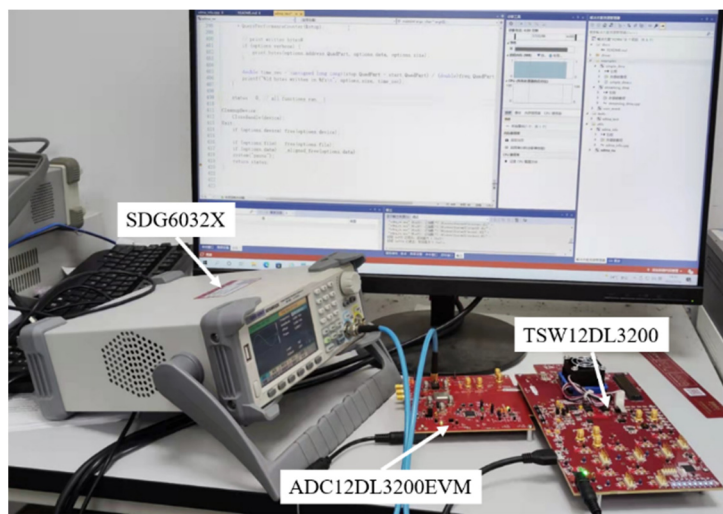


Figure 15. Experiment setup which is aimed to validate the proposed method.

Table 5. The features of experimental equipment.

Parameter	Test Conditions	Typical Values	Unit
The effective number of bits (ENOB)	The input frequency is 2482 MHz (dual-channel mode)	8.0	Bits
Resolution	Resolution with no missing codes	12	Bits
Differential nonlinearity (DNL)	Maximum positive excursion from the ideal step size	0.3	LSB
	Maximum negative excursion from the ideal step size	-0.3	
Integral nonlinearity (INL)	Maximum positive excursion from the ideal transfer function	1.6	LSB
	Maximum negative excursion from the ideal transfer function	-2.0	
Analog differential input full-scale range	Default	800	mV

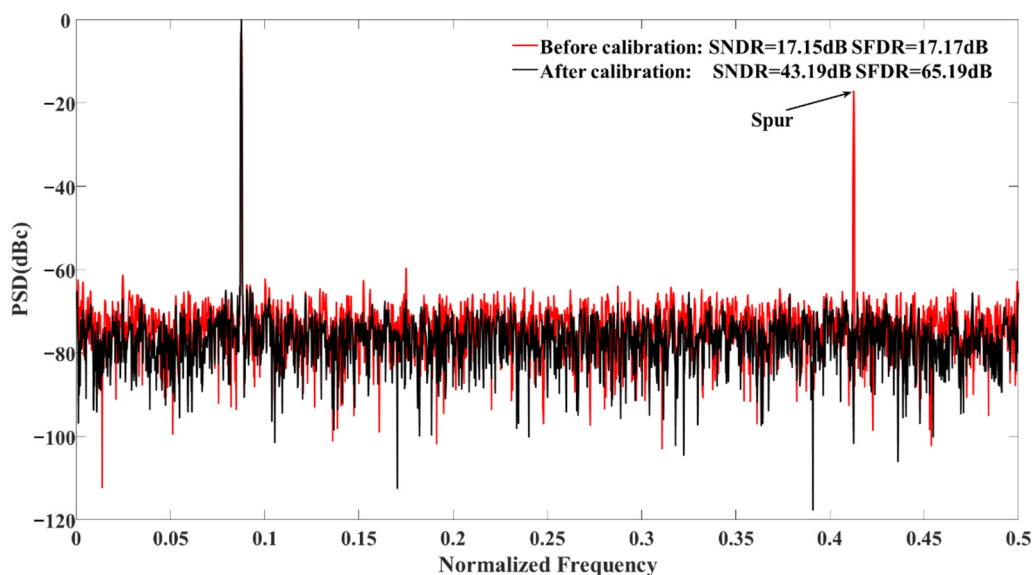


Figure 16. The frequency spectrum of the commercial 2-channel TI-ADCs before and after calibration.

In Table 6, the calibration effects of [13,16,27,30,31], and this paper are shown. After calibration, there is the highest ENOB in the proposed technique compared with [13,16,27,30,31]. Figure 16 shows the frequency spectrum of the commercial 2-channel TI-ADCs before and after calibration for the two-tone sinusoidal signals. The frequencies of the input signal are 70 MHz and 170 MHz. As shown in Figure 17, the SNDR and SFDR are respectively 11.83 dB and 10.03 dB. Additionally, the SNDR and SFDR are, respectively, 42.38 dB and 56.35 dB after calibration by the proposed algorithm. Therefore, the proposed algorithm also has a good calibration effect for actual two-tone signals.

Table 6. Comparison of calibration effects in the ADC12DL3200EVM.

	[13] Work	[16] Work	[27] Work	[30] Work	[31] Work	This Work
SNDR improvement (dB)	15.30	22.68	22.48	11.43	16.16	26.04
SFDR improvement (dB)	16.18	40.65	40.38	11.74	17.26	48.02
The effective number of bits (bit)	5.10	6.33	6.29	4.51	5.24	6.88

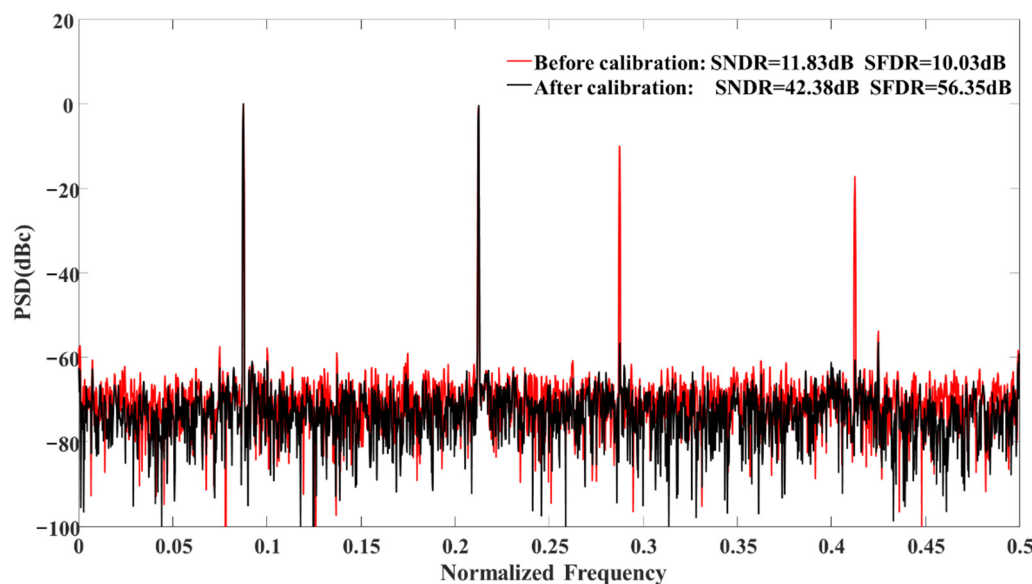


Figure 17. The frequency spectrum of the two-tone signals in the commercial 2-channel TI-ADCs before and after calibration.

5. Conclusions

This paper presents an all-digital digital background technology for the gain, time skew, and bandwidth mismatch in an M -channel under-sampling time-interleaved analog-to-digital converters (TI-ADCs) system. First, in the proposed technology, the calibration of the gain, time skew, and bandwidth mismatch is performed simultaneously. Secondly, the proposed approach enables a wide range of time skew mismatch compensation. This is an extraordinary capability that many digital calibration techniques, which use the Taylor series do not possess. Then, the proposed technique can work for ultra-high frequency signals by the bandpass fractional delay filter. Next, fewer computing resources are used to correct the input signal after obtaining the proposed parameter vector than the techniques that use the derivative filter or Hilbert filter. After that, solving a system of linear equations is used to replace matrix inversions because implementing matrix inversions within FPGA is complex. In the end, the measurement result showed that the proposed technique has a good effect on the calibration of time skew.

Author Contributions: Conceptualization, P.Y. and M.H.; methodology, P.Y.; software, M.H.; validation, P.Y. and M.H.; formal analysis, M.H.; investigation, M.H.; resources, P.Y.; data curation, M.H.; writing—original draft preparation, M.H.; writing—review and editing, M.H.; visualization, M.H.; supervision, P.Y.; project administration, P.Y.; funding acquisition, P.Y. All authors have read and agreed to the published version of the manuscript.

Funding: This research was funded by the project under the national key research and development plan, China, grant number [2018YFB2003303].

Institutional Review Board Statement: Not applicable.

Informed Consent Statement: Not applicable.

Data Availability Statement: There are no publicly archived datasets analyzed or generated during the study.

Conflicts of Interest: The authors declare no conflict of interest.

Abbreviations

TI-ADCs	Time-interleaved analog-to-digital converters
LS	Least squares
ADCs	Analog-to-digital converters
SAR	Successive-approximation-register
ADC	Analog-to-digital converter
FPGA	Field-programmable gate array
WSS	Wide-sense stationary
DTFT	Discrete-time Fourier Transform
IDTFT	Inverse discrete-time Fourier transform
SNDR	Signal-to-noise distortion ratio
SFDR	Spurious-free dynamic Rrange

References

1. Jiang, W.; Zhu, Y.; Zhang, M.; Chan, C.-H.; Martins, R.P. A Temperature-Stabilized Single-Channel 1-GS/s 60-dB SNDR SAR-Assisted Pipelined ADC With Dynamic Gm-R-Based Amplifier. *IEEE J. Solid-State Circuits* **2020**, *55*, 322. [[CrossRef](#)]
2. Black, W.C.; Hodges, D.A. Time Interleaved Converter Arrays. *IEEE J. Solid-State Circuits* **1980**, *15*, 1022. [[CrossRef](#)]
3. Seong, K.; Jung, D.-K.; Yoon, D.-H.; Han, J.-S.; Kim, J.-E.; Kim, T.T.-H.; Lee, W.; Baek, K.-H. Time-Interleaved SAR ADC with Background Timing-Skew Calibration for UWB Wireless Communication in IoT Systems. *Sensors* **2020**, *20*, 2430. [[CrossRef](#)] [[PubMed](#)]
4. Zhang, J.; Zhou, Y.; Zhao, J.; Niu, G.; Luo, X. Joint Error Estimation and Calibration Method of Memory Nonlinear Mismatch for a Four-Channel 16-Bit TIADC System. *Sensors* **2022**, *22*, 2427. [[CrossRef](#)] [[PubMed](#)]
5. Ghosh, S.; Sahoo, B.D. Closed-Form Expression for the Combined Effect of Offset, Gain, Timing, and Bandwidth Mismatch in Time-Interleaved ADCs Using Generalized Sampling. *IEEE Trans. Instrum. Meas.* **2021**, *70*, 1–12. [[CrossRef](#)]
6. Ding, H.; Wu, D.; Zheng, X.; Zhou, L.; Chen, T.; Lv, F.; Wang, J.; An, B.; Wu, J.; Liu, X. A Low-Distortion 20 GS/s Four-Channel Time-Interleaved Sample-and-Hold Amplifier in 0.18 μm SiGe BiCMOS. *Electronics* **2020**, *9*, 20. [[CrossRef](#)]
7. Adiyaman, M.Y.; Karalar, T.C. Time-interleaved SAR ADC design with background calibration. *Int. J. Circuit Theory Appl.* **2020**, *48*, 321–334. [[CrossRef](#)]
8. Su, C.K.; Hurst, P.J.; Lewis, S.H. A Time-Interleaved SAR ADC With Signal-Independent Background Timing Calibration. *IEEE Trans. Circuits Syst. I Regul. Pap.* **2022**, *69*, 620. [[CrossRef](#)]
9. Chang, D.-J.; Choi, M.; Ryu, S.-T. A 28-nm 10-b 2.2-GS/s 18.2-mW Relative-Prime Time-Interleaved Sub-Ranging SAR ADC With On-Chip Background Skew Calibration. *IEEE J. Solid-State Circuits* **2021**, *56*, 2691. [[CrossRef](#)]
10. Järvinen, O.; Kemp, I.; Unnikrishnan, V.; Stadius, K.; Kosunen, M.; Ryyränen, J. Fully Digital On-Chip Wideband Background Calibration for Channel Mismatches in Time-Interleaved Time-Based ADCs. *IEEE Solid-State Circuits Lett.* **2022**, *5*, 9. [[CrossRef](#)]
11. Niu, H.; Yuan, J. A Spectral-Correlation-Based Blind Calibration Method for Time-Interleaved ADCs. *IEEE Trans. Circuits Syst. I Regul. Pap.* **2020**, *67*, 5007. [[CrossRef](#)]
12. Jiang, W.; Zhu, Y.; Chan, C.H.; Murmann, B.; Martins, R.P. A 7-bit 2 GS/s Time-Interleaved SAR ADC With Timing Skew Calibration Based on Current Integrating Sampler. *IEEE Trans. Circuits Syst. I Regul. Pap.* **2021**, *68*, 557. [[CrossRef](#)]
13. Liu, S.; Zhao, L.; Li, S. A Novel All-Digital Calibration Method for Timing Mismatch in Time-Interleaved ADC Based on Modulation Matrix. *IEEE Trans. Circuits Syst. I Regul. Pap.* **2022**, *69*, 2955. [[CrossRef](#)]

14. Guo, M.; Mao, J.; Sin, S.-W.; Wei, H.; Martins, R.P. A 1.6-GS/s 12.2-mW Seven-/Eight-Way Split Time-Interleaved SAR ADC Achieving 54.2-dB SNDR With Digital Background Timing Mismatch Calibration. *IEEE J. Solid-State Circuits* **2020**, *55*, 693. [[CrossRef](#)]
15. Lu, Z.; Tang, H.; Ren, Z.; Hua, R.; Zhuang, H.; Peng, X. A Timing Mismatch Background Calibration Algorithm with Improved Accuracy. *IEEE Trans. Very Large Scale Integr. (VLSI) Syst.* **2021**, *29*, 1591. [[CrossRef](#)]
16. Ta, V.-T.; Hoang, V.-P.; Pham, V.-P.; Pham, C.-K. An Improved All-Digital Background Calibration Technique for Channel Mismatches in High Speed Time-Interleaved Analog-to-Digital Converters. *Electronics* **2020**, *9*, 73. [[CrossRef](#)]
17. Lan, J.; Zhai, D.; Chen, Y.; Ni, Z.; Shen, X.; Ye, F.; Ren, J. A 2.5-GS/s Four-Way-Interleaved Ringamp-Based Pipelined-SAR ADC with Digital Background Calibration in 28-nm CMOS. *Electronics* **2021**, *10*, 3173. [[CrossRef](#)]
18. Liu, X.; Xu, H.; Johansson, H.; Wang, Y.; Li, N. Correlation-Based Calibration for Nonlinearity Mismatches in Dual-Channel TIADCs. *IEEE Trans. Circuits Syst. II Express Briefs* **2020**, *67*, 585. [[CrossRef](#)]
19. Tavares, Y.A.; Lee, M. A Foreground Calibration for M-Channel Time-Interleaved Analog-to-Digital Converters Based on Genetic Algorithm. *IEEE Trans. Circuits Syst. I Regul. Pap.* **2021**, *68*, 1444. [[CrossRef](#)]
20. Miki, T.; Ozeki, T.; Naka, J. A 2-GS/s 8-bit Time-Interleaved SAR ADC for Millimeter-Wave Pulsed Radar Baseband SoC. *IEEE J. Solid-State Circuits* **2017**, *52*, 2712. [[CrossRef](#)]
21. Park, Y.; Kim, J.; Kim, C. A Scalable Bandwidth Mismatch Calibration Technique for Time-Interleaved ADCs. *IEEE Trans. Circuits Syst. I Regul. Pap.* **2016**, *63*, 1889. [[CrossRef](#)]
22. Lin, C.-Y.; Lee, T.-C. A 12-bit 210-MS/s 2-Times Interleaved Pipelined-SAR ADC With a Passive Residue Transfer Technique. *IEEE Trans. Circuits Syst. I Regul. Pap.* **2016**, *63*, 929. [[CrossRef](#)]
23. Stepanovic, D.; Nikolic, B. A 2.8 GS/s 44.6 mW Time-Interleaved ADC Achieving 50.9 dB SNDR and 3 dB Effective Resolution Bandwidth of 1.5 GHz in 65 nm CMOS. *IEEE J. Solid-State Circuits* **2013**, *48*, 971. [[CrossRef](#)]
24. Song, J.; Ragab, K.; Tang, X.; Sun, N. A 10-b 800-MS/s Time-Interleaved SAR ADC With Fast Variance-Based Timing-Skew Calibration. *IEEE J. Solid-State Circuits* **2017**, *52*, 2563. [[CrossRef](#)]
25. El-Chammas, M.; Murmann, B. A 12-GS/s 81-mW 5-bit Time-Interleaved Flash ADC With Background Timing Skew Calibration. *IEEE J. Solid-State Circuits* **2011**, *46*, 838. [[CrossRef](#)]
26. Le Duc, H. All-Digital Calibration of Timing Skews for TIADCs Using the Polyphase Decomposition. *IEEE Trans. Circuits Syst. II Express Briefs* **2016**, *63*, 99. [[CrossRef](#)]
27. Qiu, Y.; Liu, Y.-J.; Zhou, J.; Zhang, G.; Chen, D.; Du, N. All-Digital Blind Background Calibration Technique for Any Channel Time-Interleaved ADC. *IEEE Trans. Circuits Syst. I Regul. Pap.* **2018**, *65*, 2503. [[CrossRef](#)]
28. Ta, V.T.; Hoang, V.P.; Tran, X.N. All-Digital Background Calibration Technique for Offset, Gain and Timing Mismatches in Time-Interleaved ADCs. *EAI Endorsed Trans. Ind. Netw. Intell. Syst.* **2019**, *19*, 21. [[CrossRef](#)]
29. Jun, J. A condensed Cramer's rule for the minimum norm least-squares solution of linear equations. *Linear Algebra Its Appl.* **2012**, *437*, 9. [[CrossRef](#)]
30. Li, D.; Zhu, Z.; Ding, R.; Liu, M.; Yang, Y.; Sun, N. A 10-Bit 600-MS/s Time-Interleaved SAR ADC With Interpolation-Based Timing Skew Calibration. *IEEE Trans. Circuits Syst. II Express Briefs* **2019**, *66*, 16–24. [[CrossRef](#)]
31. Yin, M.; Ye, Z. First Order Statistic Based Fast Blind Calibration of Time Skews for Time-Interleaved ADCs. *IEEE Trans. Circuits Syst. II Express Briefs* **2020**, *67*, 162–166. [[CrossRef](#)]